Energy Advances

ROYAL SOCIETY OF CHEMISTRY

PAPER

View Article Online
View Journal | View Issue

Check for updates

Cite this: *Energy Adv.*, 2023, 2, 1375

An efficient oxygen evolution reaction catalyst using Ni–Co layered double hydroxide anchored on reduced graphene oxide†

Sora Wakamatsu,[a] Md. Saidul Islam, *[ab] Yuta Shudo,[c] Masahiro Fukuda,[a] Ryuta Tagawa,[a] Nonoka Goto,[a] Michio Koinuma,[b] Yoshihiro Sekine[ad] and Shinya Hayami *[abe]

An efficient oxygen evolution reaction (OER) catalyst is crucial in various electrochemical applications including renewable energy, electrochemistry, and environmental science. Herein, we report the OER performance and stability of a nonprecious metal electrocatalyst consisting of nickel and cobalt-layered double hydroxides (NiCo-LDH) and reduced graphene oxide (rGO) using hydrothermal methods. The prepared NiCo-LDH@rGO catalyst exhibits a homogeneous distribution of NiCo-LDH on the rGO surface and an excellent OER performance. The OER potential of NiCo-LDH@rGO shows a value of 1.60 V at a current density (η) of 10 mA cm^{-2}, which is 100 mV lower than that of iridium oxide (IrO_2) (η = 10 mA cm^{-2} at 1.70 V). Interestingly, at the current density of 20 mA cm^{-2}, the observed OER potentials for NiCo-LDH@rGO and IrO_2 are 1.65 and 1.84 V, respectively, indicating that NiCo-LDH@rGO has 190 mV lower overpotential compared to IrO_2. The NiCo-LDH@rGO catalyst also shows a lower value of Tafel slope (74 mV dec^{-1}) indicating faster reaction kinetics. The enhanced performance and stability of the NiCo-LDH@rGO catalyst can be attributed to the exposed active sites and the faster electron transfer, due to the synergistic effect of rGO in the NiCo-LDH, which promotes the OER oxidation process.

Received 2nd May 2023,
Accepted 8th July 2023

DOI: 10.1039/d3ya00192j

rsc.li/energy-advances

Open Access Article. Published on 13 Aywoho-Kitawonsa 2023. Downloaded on 2025/10/26 3:12:46 PM.
This article is licensed under a Creative Commons Attribution 3.0 Unported Licence.

Introduction

The oxygen evolution reaction (OER) plays a key role in determining the efficiency and performance in various electrochemical applications, such as electrocatalysis, supercapacitors, and battery technology. In particular, the OER is the key step for the efficient and sustainable generation of hydrogen through water splitting, and its use in fuel cells, energy storage, and other applications. In addition, the OER is used in the production of ozone, which is an important oxidant for water purification and treatment of industrial waste. Therefore, the development of new OER catalysts can lead toward a clean and sustainable energy future.[1–3] Unfortunately, the OER is a sluggish and energy-intensive process, and it requires a suitable catalyst to enhance its efficiency. The OER catalysts traditionally rely profoundly on the use of precious metals such as iridium oxide (IrO_2) or ruthenium oxide (RuO_2), while the high price, scarcity and limited electrocatalytic ability at high current density limit their large-scale application.[4,5] Therefore, there is a need to develop inexpensive catalysts that can be mass-produced and have optimum catalytic performance to overcome high overpotential and slow kinetics.

Layered double hydroxides (LDHs) are a class of layered materials of hydroxides composed of multiple metals. LDHs possess a unique structure that consists of positively charged layered sheets of hydroxide anions separated by interlayer anions, which makes them promising for different applications, including catalysts for OER reactions.[2] LDHs possess a combination of several factors, including a high surface area, structural stability, and electronic structure which makes LDHs a highly promising catalyst for energy conversion and storage applications. Specifically, (i) the unique composition of metal cations and hydroxyl anions provides active sites for catalytic reactions, (ii) metal cations in LDHs can promote

[a] *Department of Chemistry, Graduate School of Science and Technology, Kumamoto University, 2-39-1 Kurokami, Chuo-ku, Kumamoto 860-8555, Japan. E-mail: hayami@kumamoto-u.ac.jp*
[b] *Institute of Industrial Nanomaterials (IINa), Kumamoto University, 2-39-1 Kurokami, Chuo-ku, Kumamoto 860-8555, Japan*
[c] *National Institute of Advanced Industrial Science and Technology (AIST), Japan*
[d] *Priority Organization for Innovation and Excellence, Kumamoto University, 2-39-1 Kurokami, Chuo-ku, Kumamoto 860-8555, Japan*
[e] *International Research Center for Agricultural and Environmental Biology (IRCAEB), 2-39-1 Kurokami, Chuo-ku, Kumamoto 860-8555, Japan*

† Electronic supplementary information (ESI) available. See DOI: https://doi.org/10.1039/d3ya00192j

© 2023 The Author(s). Published by the Royal Society of Chemistry

Open Access Article. Published on 13 Aywoho-Kitawonsa 2023. Downloaded on 2025/10/26 3:12:46 PM.
This article is licensed under a Creative Commons Attribution 3.0 Unported Licence.

the adsorption of water molecules and oxygen ions, which are crucial for the catalytic process, (iii) LDHs have a high surface area, which provides more active sites for catalytic reactions and enhances their catalytic efficiency and (iv) the structural stability of the LDH as the layered structure of LDHs is stable and provides a supportive environment for the catalytic reaction to occur and allows the preservation of the active sites and prevents the deactivation of the catalyst.[2] Therefore, non-precious transition metal (such as Ni and Co)-based LDHs are expected to be a promising candidate for replacing traditional precious metal-based catalysts. However, two major factors should be considered for their optimum performance, including (a) hydrogen bonding interactions between the layered structures resulting in the particle aggregation often responsible for a low specific surface area and (b) the poor intrinsic electrical conductivity of LDHs, which is disadvantageous to the electrochemical properties, and limits their performance when used as a catalyst. The use of carbon materials as catalyst supports overcomes these limitations, and is expected to improve the LDH electrocatalytic performance toward design for a specific application.

On the other hand, graphene oxide (GO) and reduced graphene oxide (rGO) are well-studied in wide application areas in material science due to their exclusive physical and electrochemical properties.[6–14] In particular, rGO has potential as an ideal catalyst support material along with several favorable properties including (a) being a perfect platform for the hybridization of other electroactive components including metal/metal oxide NPs, and avoiding the aggregation of the nanoparticles; (b) greatly enhancing the electronic conductivity of the composite hybrids and accelerating the charge-transfer kinetics; (c) improving the dispersion of loaded catalysts, thus providing more catalytic active sites and (d) modulating the electronic structure of the active sites as a result of the synergistic interaction between the graphene moiety and loaded metals.[15] As a result, the development of a homogeneous distribution and stable interface between LDHs and rGO is expected to show unique electrochemical properties and is considered in the current work for efficient OER electrocatalysts (Scheme 1).

During the past few years, different LDH and LDH-based materials have been reported as OER electrocatalysts.[16–19] However, to the best of our knowledge, the growth of NiCo-LDH on the rGO sheets (NiCo-LDH@rGO) has not been reported to date. In this study, we develop a hybrid catalyst of NiCo-LDH and rGO

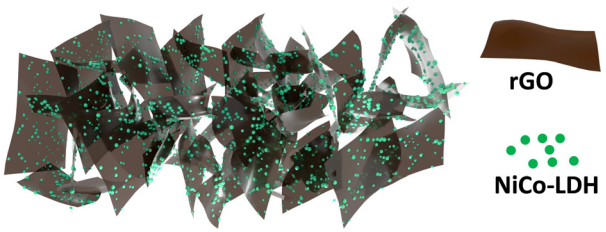

Scheme 1 Distribution of NiCo-LDH on the rGO surface.

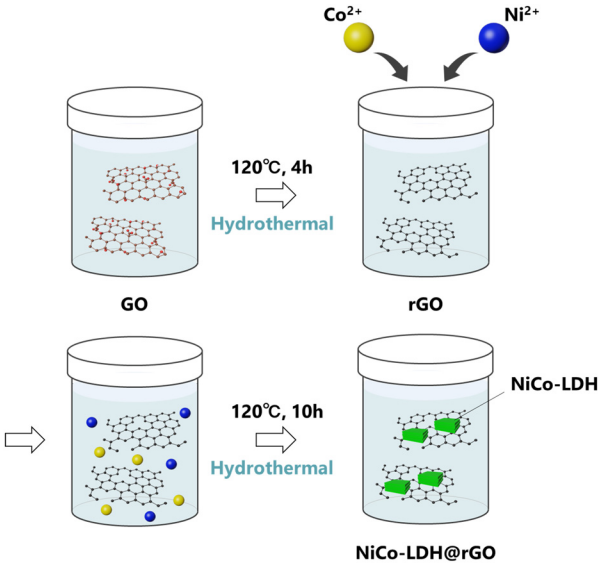

Scheme 2 Schematic illustration for preparation of the NiCo-LDH@rGO hybrid.

using a two-step hydrothermal route. In the first step, rGO is prepared followed by the NiCo-LDH grown in the rGO during the second hydrothermal step (Scheme 2). The OER performance and stability of the NiCo-LDH@rGO catalyst is measured and compared with the pure NiCo-LDH and IrO_2 catalyst. The NiCo-LDH@rGO hybrid exhibited superior OER activity and lower overvoltage compared to pure NiCo-LDH and IrO_2 catalysts.

Experimental

All reagents were of analytical grade and used without further purification.

Preparation of GO

GO was prepared from graphite through a modified Hummers' route using our previously reported work.[7] The GO dispersion was maintained at 10 mg mL^{-1} in H_2O.

Fabrication of rGO

The GO dispersion (10 mg mL^{-1}, 20 mL) was transferred to a 100 mL Teflon-lined autoclave. The autoclave was sealed and heated at 160 °C for 10 hours, then allowed to cool naturally at room temperature. It was then dried in an oven at 60 °C. In this process, rGO is obtained as a large aggregated product. Therefore, the ball milling of rGO was carried out for 6h at ambient conditions to grind the rGO into smaller particles.

Fabrication of NiCo-LDH@rGO

In a typical synthesis process, $Co(NO_3)_2{\cdot}6H_2O$ (0.291 g, 1 mmol), $Ni(NO_3)_2{\cdot}6H_2O$ (0.291 g, 1 mmol) and hexamethylenetetramine (1.68 g) were dissolved in 20 mL of DI water to form a homogenous solution. Another suspension was prepared by dispersing 20 mL of rGO (10 mg mL^{-1}). The mixture of the two

© 2023 The Author(s). Published by the Royal Society of Chemistry

Open Access Article. Published on 13 Aywoho-Kitawonsa 2023. Downloaded on 2025/10/26 3:12:46 PM.
This article is licensed under a Creative Commons Attribution 3.0 Unported Licence.

solutions was transferred to a 100 mL Teflon-lined autoclave. The autoclave was sealed and heated at 120 °C for 10 hours, then allowed to cool naturally at room temperature. It was then dried in an oven at 60 °C.

Fabrication of NiCo-LDH

The NiCo-LDH sample was produced in a similar way as for NiCo-LDH@rGO, except (i) rGO dispersion is not added and (ii) using half the amount of hexamethylenetetramine (0.82 g) for the synthesis process.

Characterization

The structure and morphology of the individual samples were characterized by powder X-ray diffraction (XRD, RigakuDmax/Ultima IV), field emission scanning electron microscopy with EDX facility (FE-SEM, JSM-7600F, JEOL), X-ray photoelectron spectroscopy (XPS, Theta Probe, Thermo Fisher Scientific) and Raman spectroscopy (NRS-3100, JASCO).

Electrochemical measurement

Electrochemical characterization was performed at room temperature using a conventional three-electrode cell equipped with a Rotating (Ring) Disk Electrode and potentiostat (RRDE-3A). 5 mg sample was ultrasonicated in 480 µl of ethanol and 20 µl of Nafion solution (0.5 wt%) for 30 minutes. Then, 5 µl of the sample dispersion was loaded on the disk electrode. All electrochemical performances were investigated in 1 M KOH solution using a Ag/AgCl electrode as the reference and a Pt wire as the counter electrode. All potentials measured were adjusted to the reversible hydrogen electrode (RHE) according to the Nernst equation:

$$E_{RHE} = E + 0.0059 \times pH + 0.199$$

Before the electrochemical measurement, the electrolyte was degassed by bubbling oxygen for at least 30 min to ensure the H_2O/O_2 equilibrium at 1.23 V (*versus* the RHE).

Results and discussion

Fig. 1 shows the surface morphology and characterization of the prepared NiCo-LDH and NiCo-LDH@rGO electrocatalysts. The FE-SEM image of rGO in Fig. S1 (ESI†) can be observed as a typical large sheet-type structure. FE-SEM images of NiCo-LDH and NiCo-LDH@rGO are shown in Fig. 1a and b, respectively. The layered structure of LDH has been confirmed in both NiCo-LDH and NiCo-LDH@rGO. The EDX mapping of NiCo-LDH and NiCo-LDH@rGO were conducted to ensure the homogeneity of the surface morphology of the prepared materials, which are shown in Fig. S2 and S3 (ESI†), respectively. In EDX mapping, the presence of Ni and Co, and O are observed for the pure NiCo-LDH structure (Fig. S2, ESI†). On the other hand, in NiCo-LDH@rGO, a homogeneous distribution of C, Ni, Co, and O, is observed, which indicates that LDH is well-grown on the rGO sheets. Fig. 1c compares the BET surface area of NiCo-LDH and NiCo-LDH@rGO. The surface area values are

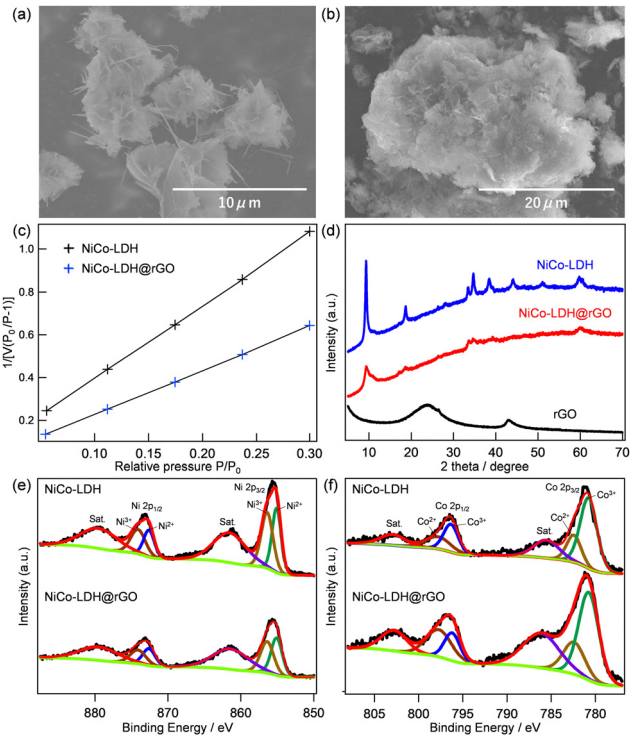

Fig. 1 Surface morphology and characterization of the prepared electrocatalyst. (a) SEM images of NiCo-LDH, (b) SEM image of NiCo-LDH@GO, (c) BET surface area of NiCo-LDH and NiCo-LDH@GO, (d) PXRD pattern for rGO, NiCo-LDH, and NiCo-LDH@GO. (e) Ni 2p XPS peak for NiCo-LDH and NiCo-LDH@GO, and (f) Co 2p XPS peak for NiCo-LDH and NiCo-LDH@GO.

28 and 46 $m^2\ g^{-1}$, for NiCo-LDH and NiCo-LDH@rGO, respectively.

The XRD patterns in Fig. 1d represent the peaks observed for rGO, NiCo-LDH, and NiCo-LDH@rGO. The diffraction pattern of GO exhibits a sharp peak centered at $2\theta = 10.3°$, which corresponds to the (001) reflection of graphite oxide.[20] The disappearance of the (001) peak and the emergence of a new diffraction peak at $2\theta = 24°$ in the XRD pattern of rGO demonstrates that graphite oxide has been well reduced.[20] The NiCo-LDH sample exhibits five characteristic diffraction peaks at 2θ values of 11.1°, 22.1°, 34.4°, 38.6°, and 60.7°, which can be indexed to the (003), (006), (009), (015) and (110) planes of hydrotalcite-like LDH phase in good agreement with previous reports.[21,22] The XRD pattern of the NiCo-LDH@rGO catalyst retains the corresponding peaks of pure NiCo-LDH, revealing the existence of NiCo-LDH in the composite without affecting the crystalline phase of LDH. The co-existence of NiCo-LDH and rGO in the NiCo-LDH@rGO has also been ensured from the Raman spectra, which are shown in Fig. S4 (ESI†). The NiCo-LDH@rGO shows the characteristics of the Raman peaks for both the NiCo-LDH phase and the rGO phase.

The chemical and electronic states of Ni and Co in NiCo-LDH and NiCo-LDH@rGO were obtained from XPS analysis. The XPS survey spectra of NiCo-LDH and NiCo-LDH@rGO are shown in Fig. S5a and S5b (ESI†), respectively. The existence of Ni, Co, C, and O elements in the NiCo-LDH@rGO is

Open Access Article. Published on 13 Aywoho-Kitawonsa 2023. Downloaded on 2025/10/26 3:12:46 PM.
This article is licensed under a Creative Commons Attribution 3.0 Unported Licence.

consistent with EDX analysis. Fig. 1e and f compare the deconvoluted Ni 2p and Co 2p spectrum, respectively, for NiCo-LDH and NiCo-LDH@rGO. In Fig. 1e, the co-existence of two kinds of nickel species (Ni^{2+} and Ni^{3+}) is observed for both samples.[23,24] Besides two shakeup satellite peaks at 879.4 eV and 861.4 eV (indicated as "Sat."), there are two major peaks at 855.5 and 873.1 eV, corresponding to Ni $2p_{3/2}$ and Ni $2p_{1/2}$, respectively. In particular, the peaks at 872.7 and 855.5 eV are consistent with Ni^{3+} and the peaks situated at 873.1 and 856.1 eV are attributed to Ni^{2+}, which indicates the presence of Ni^{3+} and Ni^{2+} in NiCo-LDH@rGO. Similarly, the Co species was confirmed to be mixed valence states of both Co^{2+} and Co^{3+} (Fig. 1f). The Co 2p spectrum can be fitted with two spin–orbit doublets and two shake-up satellites (identified as "Sat.") by using a Gaussian fitting method. One pair of binding energies centered at 780.2 and 795.6 eV corresponds to Co^{3+}, while the other pair at the higher energies of 782.1 and 796.6 eV is ascribed to Co^{2+}. These results confirmed that in both samples there exist two kinds of cobalt oxidation states in the composite: *i.e.* Co^{2+} and Co^{3+}. It is expected that the solid-state redox couples of Ni^{2+}/Ni^{3+} and Co^{2+}/Co^{3+} in NiCo-LDH and NiCo-LDH@rGO may provide an enhanced electrochemical performance because Ni^{3+} and Co^{3+} cations have been regarded as the catalytically active centers for the OER. In addition, no difference in the Ni^{2+}/Ni^{3+} and Co^{2+}/Co^{3+} ratios in NiCo-LDH and NiCo-LDH@rGO indicates that hybridization does not affect the composition of LDH.

The electrocatalytic properties of the prepared NiCo-LDH@rGO electrocatalysts were investigated in a typical three-electrode configuration in 1 M KOH aqueous solution. The loading mass of NiCo-LDH@rGO is $\sim$0.7 mg cm^{-2}. The observed results are compared with NiCo-LDH and standard IrO_2 with the same mass loading and are shown in Fig. 2. The CV curves of NiCo-LDH, NiCo-LDH @rGO, and IrO_2 with voltages ranging between 0 and 0.5 V and scan rates ranging from 5 to 100 mV s^{-1} are shown in Fig. 2a–c, respectively. In all cases, the CV curve areas increased as the scan rate increased from 5 to 100 mV s^{-1} while maintaining its shape indicating the rapid rates of ionic and electronic transfer. On the other hand, the area of the CV curve at a particular scan rate of the three materials shows the increasing order of NiCo-LDH < IrO_2 < NiCo-LDH@rGO. Compared to the CV curve areas of NiCo-LDH and IrO_2, the CV curve area of NiCo-LDH@rGO increases at each scan rate indicating the enhancement of the electrical conductivity. Fig. 2d exhibits representative linear sweep voltammetry (LSV) curves of NiCo-LDH, NiCo-LDH@rGO, and IrO_2 catalysts at a scan rate of 5 mV s^{-1}. Clearly, the OER catalytic activity of NiCo-LDH@rGO is much better than that of other catalysts. The OER catalytic activity shows the increasing order of rGO ≪ NiCo-LDH ≪ IrO_2 < NiCo-LDH@rGO. In particular,

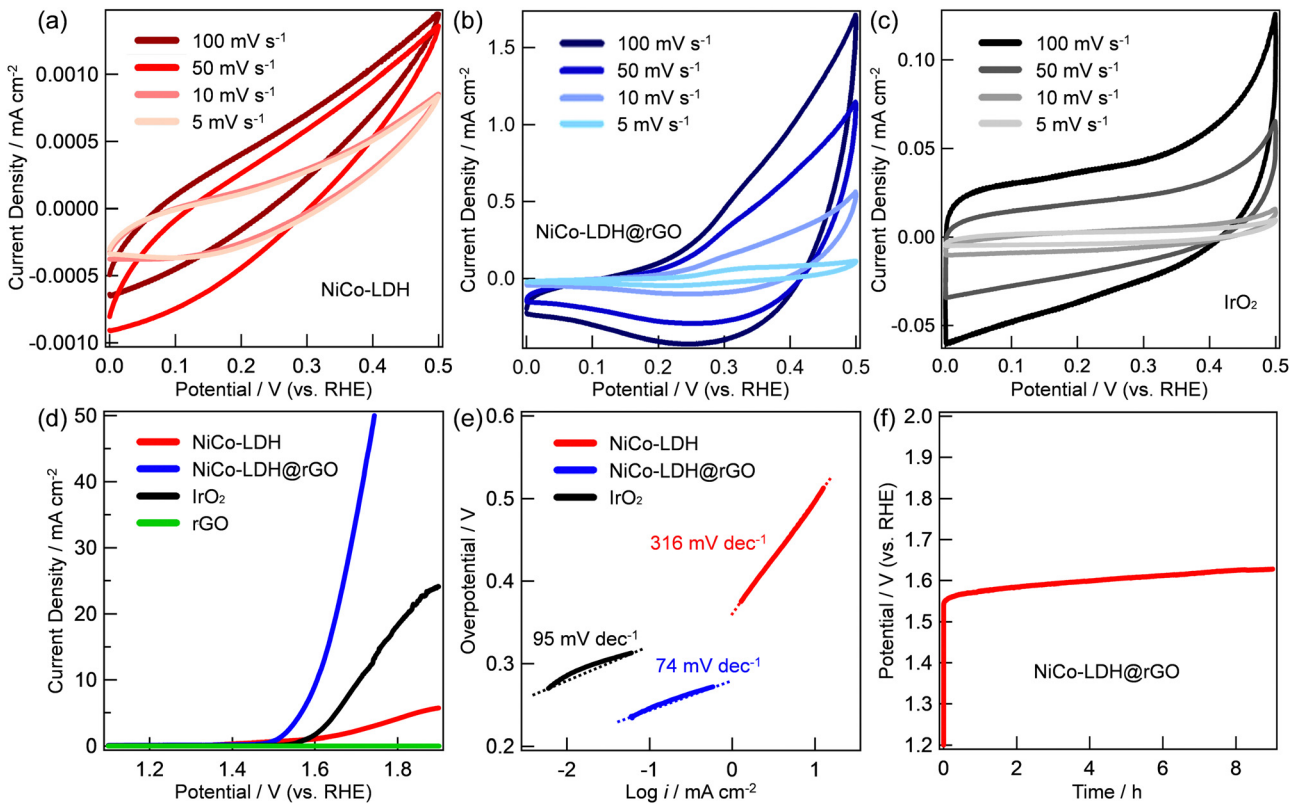

Fig. 2 Electrocatalytic OER performance of the prepared electrocatalyst. CV curves conducted at voltages ranging between 0 and 0.5 V and scan rates ranging from 5 to 100 mV s^{-1} of (a) NiCo-LDH, (b) NiCo-LDH@rGO, and (c) IrO_2. (d) Linear sweep voltammetry polarization curves of rGO, NiCo-LDH, NiCo-LDH@rGO, and IrO_2 at 1 M KOH during OER testing. (e) Tafel plot of NiCo-LDH, NiCo-LDH@rGO, and IrO_2 towards the OER, and (f) chronopotentiometry (time-dependence of the potential) for NiCo-LDH@rGO conducted under 1 M KOH at 5 mA cm^{-2} indicating the stability.

© 2023 The Author(s). Published by the Royal Society of Chemistry

Open Access Article. Published on 13 Aywoho-Kitawonsa 2023. Downloaded on 2025/10/26 3:12:46 PM.
This article is licensed under a Creative Commons Attribution 3.0 Unported Licence.

Table 1 Reported OER performance for some LDH-based catalysts

OER catalyst	Onset potential (V)	Overpotential (10 mA cm^{-2})	Tafel slope	Ref.
ZnCo-LDH NS	1.55	385	108	16
MnNi-LDH	1.57	420	79.7	17
CoMn-LDH	—	395	45	18
$Co(OH)_2$@rGONF	1.52	417	57	19
NiCo-LDH@rGO	1.46	376	74	This work

in the case of NiCo-LDH@rGO, the OER oxidation current was observed (onset potential) at 1.46 V and reached 10 mA cm^{-2} at 1.60 V. The current density was sharply increased to 20 mA cm^{-2} at 1.65 V. On the other hand, the current density of 10 and 20 mA cm^{-2} was observed at 1.65 and 1.84 V, respectively for IrO_2. The observed overpotentials are 376 mV and 460 mV at a current density of 10 mA cm^{-2} for NiCo-LDH@rGO and IrO_2, respectively, while the respective overpotentials are 420 and 610 mV at the current density of 20 mA cm^{-2}. The observed OER performance of NiCo-LDH is much less than that of NiCo-LDH@rGO and IrO_2. The corresponding Tafel slopes of the catalysts are shown in Fig. 1e. The Tafel slope values are calculated as 316, 95, and 74 mV dec^{-1} for NiCo-LDH, IrO_2, and NiCo-LDH@rGO, respectively, indicating a faster kinetics associated with the NiCo-LDH@rGO compared to that of IrO_2 and NiCo-LDH. Finally, the stability of the NiCo-LDH@rGO catalyst was conducted by performing the chronopotentiometry at a current density of 5 mA cm^{-2} (Fig. 1f). The catalyst maintained an almost stable potential of about 1.6 V over 9 h.

The improvement in OER performance may be due to several reasons including (i) higher surface area of NiCo-LDH@rGO and the homogeneous dispersion of NiCo-LDH on the surface of rGO (confirmed from N_2 adsorption–desorption and the EDX mapping in Fig. 1c and Fig. S3, ESI† respectively) which can expose many active sites enhancing the OER performance, (ii) rGO has a positive effect on preventing the restacking of NiCo-LDH, and (iii) the introduction of rGO improves the electrical conductivity of NiCo-LDH and provide strong chemical and electronic coupling between NiCo-LDH and rGO.[25] Furthermore, the electrochemical active surface areas (ECSAs) of NiCo-LDH and NiCo-LDH@rGO are obtained based on the electrochemical double-layer capacitance (C_{dl}) through CV at different scan rates (5, 10, 30, 50, 80, and 100 mV s^{-1}) with voltages ranging between 1.025 and 1.120 V *vs.* RHE, where there was no faradaic current. The obtained ECSA values of NiCo-LDH and NiCo-LDH@rGO are 0.57 and 373, respectively. This indicated that NiCo-LDH@rGO exposed more catalytically active electrolysis sites, exhibiting higher OER catalytic activity. Table 1 compares the reported OER onset potential, overpotential, and Tafel slope values for some reported LDH-based materials and the results obtained from NiCo-LDH@rGO. Clearly, NiCo-LDH@rGO shows an enhanced OER performance and stability compared to some previously reported LDH-based OER catalysts signifying the potential and possible use in practical applications.

Conclusions

In summary, NiCo-LDH@rGO was successfully prepared using a hydrothermal route while NiCo-LDH was homogeneously distributed to the rGO surface. The electrochemical OER measurement of NiCo-LDH@rGO suggests an excellent catalytic property of the overpotential of only 376 mV at a current density of 10 mA cm^{-2}. Furthermore, a significant reduction in overpotential at about 190 mV was observed compared to the IrO_2 catalyst at the current density of 20 mA cm^{-2}. The calculated Tafel slope of NiCo-LDH@rGO is 74 mV dec^{-1}. The superior OER electrochemical performance of the NiCo-LDH@rGO nanocomposite can be attributed to the merits of the high electrochemical activity of NiCo-LDH together with the high electronic conductivity of rGO and the synergistic effect of NiCo-LDH and rGO components to prevent self-aggregation. The hybridization method is also vital as LDH is grown on rGO by hydrothermal synthesis to reduce the resistance at the LDH-rGO interface and enable smooth electron transfer. Therefore, the NiCo-LDH@rGO OER catalyst, synthesized from the economic and earth-abundant elements, shows great potential as a low-cost alternative to the noble IrO_2 or RuO_2 catalysts.

Conflicts of interest

There are no conflicts to declare.

Acknowledgements

This work was supported by the Kakenhi Grant-in-Aid for Challenging Research (Exploratory) JP20K21213.

Notes and references

1 F. Zeng, C. Mebrahtu, L. Liao, A. K. Beine and R. Palkovits, *J. Energy Chem.*, 2022, **69**, 301.
2 D. Zhou, P. Li, X. Lin, A. McKinley, Y. Kuang, W. Liu, W.-F. Lin, X. Sun and X. Duan, *Chem. Soc. Rev.*, 2021, **50**, 8790.
3 A. Vazhayil, L. Vazhayal, J. Thomas, C. S. Ashok and N. Thomas, *Appl. Surface Sci. Adv.*, 2021, **6**, 100184.
4 H. N. Nong, L. Gan, E. Willinger, D. Teschner and P. Strasser, *Chem. Sci.*, 2014, **5**, 2955.
5 T. Reier, Z. Pawolek, S. Cherevko, M. Bruns, T. Jones, D. Teschner, S. Selve, A. Bergmann, H. N. Nong, R. Schlögl, K. J. J. Mayrhofer and P. Strasser, *J. Am. Chem. Soc.*, 2015, **137**, 13031.
6 M. Fukuda, M. S. Islam, R. Shimizu, H. Nasser, N. N. Rabin, Y. Takahashi, Y. Sekine, L. F. Lindoy, T. Fukuda and T. Ikeda, *ACS Appl. Nano Mater.*, 2021, **4**, 11881.
7 M. Fukuda, M. S. Islam, Y. Shudo, J. Yagyu, L. F. Lindoy and S. Hayami, *Chem. Commun.*, 2020, **56**, 4364–4367.

© 2023 The Author(s). Published by the Royal Society of Chemistry

Open Access Article. Published on 13 Aywoho-Kitawonsa 2023. Downloaded on 2025/10/26 3:12:46 PM.
This article is licensed under a Creative Commons Attribution 3.0 Unported Licence.

8 M. S. Islam, M. R. Karim, S. Islam, J. Kim, N. N. Rabin, R. Ohtani, M. Nakamura, M. Koinuma and S. Hayami, *ChemistrySelect*, 2016, **1**, 6429.
9 M. S. Islam, J. Yagyu, Y. Sekine, S. Sawa and S. Hayami, *Mater. Adv.*, 2022, **3**, 3418.
10 M. R. Karim, M. S. Islam, K. Hatakeyama, M. Nakamura, R. Ohtani, M. Koinuma and S. Hayami, *J. Phys. Chem. C*, 2016, **120**, 21976.
11 Y. Shudo, M. S. Islam, M. R. Karim, N. N. Rabin, K. Wakata, R. Ohtani, M. Nakamura, L. F. Lindoy and S. Hayami, *Global Challenges*, 2017, **1**, 1700054.
12 M. Tsutsumi, M. S. Islam, M. R. Karim, N. N. Rabin, R. Ohtani, M. Nakamura, L. F. Lindoy and S. Hayami, *Bull. Chem. Soc. Jpn.*, 2017, **90**, 950.
13 J. Yagyu, M. S. Islam, Y. Shudo, M. Fukuda, H. Ushijima, J. Ohyama, S. Ida, L. F. Lindoy and S. Hayami, *ACS Appl. Energy Mater.*, 2021, **4**, 6296.
14 J. Yagyu, M. S. Islam, H. Yasutake, H. Hirayama, H. Zenno, A. Sugimoto, S. Takagi, Y. Sekine, S.-I. Ohira and S. Hayami, *Bull. Chem. Soc. Jpn.*, 2022, **95**, 862.
15 M. S. Islam, Y. Shudo and S. Hayami, *Bull. Chem. Soc. Jpn.*, 2022, **95**, 1.
16 C. Qiu, F. Cai, Y. Wang, Y. J. Liu, Q. Wang and C. Zhao, *J. Colloid Interface Sci.*, 2020, **565**, 351.
17 E. Jung, J. K. Kim, H. Choi, M. H. Lee and T. Yu, *Dalton Trans.*, 2018, **47**, 17342.
18 Z. Yi, C. Ye, M. Zhang, Y. Lu, Y. Liu, L. Zhang and K. Yan, *Appl. Surf. Sci.*, 2019, **480**, 256.
19 B. Rezaei, A. R. T. Jahromi and A. A. Ensafi, *Int. J. Hydrogen Energy*, 2017, **42**, 16538.6.
20 M. S. Islam, H. Ohmagari, M. A. Rahman, M. Fukuda, Y. Shudo, J. Yagyu, Y. Sekine, L. F. Lindoy and S. Hayami, *Mater. Adv.*, 2021, **2**, 5645.
21 J. C. Huang, T. Lei, X. P. Wei, X. W. Liu, T. Liu, D. X. Cao, J. L. Yin and G. L. Wang, *J. Power Sources*, 2013, **232**, 370.
22 H. Xu, J. Wu, J. Liu, Y. Chen and X. Fan, *J. Mater. Sci.: Mater. Electron.*, 2018, **29**, 17234.
23 K. S. Kim, N. M. Shinde, J. M. Yun and K. H. Kim, *RSC Adv.*, 2021, **11**, 12449.
24 W. Tian, J. Zhang, H. Feng, H. Wen, X. Sun, X. Guan, D. Zheng, J. Liao, M. Yan and Y. Yao, *Sustainable Energy Fuels*, 2021, **5**, 391.
25 X. Cai, X. Shen, L. Ma, Z. Ji, C. Xu and A. Yuan, *Chem. Eng. J.*, 2015, **268**, 51.

© 2023 The Author(s). Published by the Royal Society of Chemistry